ACS APPLIED MATERIALS & INTERFACES

Research Article

www.acsami.org

Citrate-Free Synthesis of Silver Nanoplates and the Mechanistic Study

Qiang Zhang,[†] Yin Yang,[†] Jonathan Li,[†] Raymond Iurilli,[†] Shuifen Xie,[‡] and Dong Qin*,[†]

[†]School of Materials Science and Engineering, Georgia Institute of Technology, Atlanta, Georgia 30332, United States

[‡]The Wallace H. Coulter Department of Biomedical Engineering, Georgia Institute of Technology and Emory University, Atlanta, Georgia 30332, United States

Supporting Information

ABSTRACT: We report a citrate-free synthesis of Ag nanoplates with an edge length of 50 nm that involved the reduction of $AgNO_3$ by poly(vinyl pyrrolidone) (PVP) in ethanol at 80 °C under a solvothermal condition. Within a period of 4 h, greater than 99% of the initially added $AgNO_3$ could be converted into Ag nanoplates with excellent stability. To understand this remarkably simple and efficient process, we systematically investigated the roles played by various reaction parameters, which include the type of precursor, reducing powers of PVP and ethanol, molar ratio of PVP to $AgNO_3$, solvent, involvement of O_2, and effects of pressure and temperature. Our results suggest a plausible mechanism that involves (i) fast reduction of $AgNO_3$ to generate Ag multiple twinned particles (MTPs) via a thermodynamically controlled process, (ii) kinetically controlled formation of plate-like seeds and their further growth into small nanoplates in the presence of Ag^+ ions at a low concentration, and (iii) complete transfer of Ag atoms from the MPTs to nanoplates via O_2-mediated Ostwald ripening. We demonstrated that the molar ratio of PVP to $AgNO_3$ in ethanol plays an essential role in controlling the reduction rate for the formation of MTPs and plate-like seeds under the solvothermal condition, transformation kinetics, and final morphology taken by the Ag nanoplates. In particular, when the reaction temperatures were above the boiling point of ethanol, the pressure induced by a solvothermal process accelerated the oxidative etching of Ag MTPs to facilitate their complete conversion into nanoplates. The mechanistic insight could serve as a guideline to optimize the experimental parameters of a solvothermal synthesis to control the reduction kinetics and thus the formation of metallic nanocrystals with controlled shapes and in high yields and large quantities.

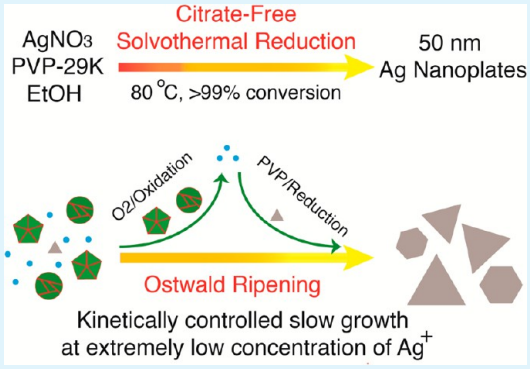

KEYWORDS: *silver nanoplates, solvothermal synthesis, Ostwald ripening, surface plasmon resonance*

INTRODUCTION

Silver nanoplates, a good example of two-dimensional nanostructures, exhibit an extreme degree of anisotropy in their shape and unique features in their localized surface plasmon resonances (LSPR) properties.[1−3] Many groups have demonstrated that the size, shape, and morphology of Ag nanoplates can all be maneuvered to tailor their LSPR properties for a variety of applications in chemical/biological sensing and imaging.[4−7] However, it remains a challenge to systematically and reproducibly control the production of Ag nanoplates. Part of the difficulty arises from the limited success in deviating the reaction from a thermodynamically controlled to a kinetically controlled pathway. In general, the metal atoms have to be kept at an extremely low concentration in order to generate plate-like seeds with stacking faults and subsequently ensure their growth into Ag nanoplates.[8]

Silver nanoplates can be prepared using a number of different protocols that involve either light-mediated reduction or direct chemical reduction. Mirkin and coworkers were the first to use light as a driving force to convert Ag nanospheres into nanoplates.[9,10] Brus and coworkers later elucidated the mechanism responsible for the photo-induced reduction of Ag^+ ions into Ag atoms.[11,12] Whereas photo-induced reactions embrace a capacity to generate Ag nanoplates on a relatively large scale with high efficiency, reproducibility remains an issue due to the absence of a mechanism that can unambiguously explain the unusual transformation from Ag nanospheres to nanoplates. Alternatively, direct chemical reduction has served as a popular approach to the production of Ag nanoplates. In 2002, Chen and Carroll reported the formation of Ag nanoplates with edge length between 40 and 300 nm via the reduction of Ag^+ ions with ascorbic acid on Ag seeds (<5 nm in diameter) in the presence of cetyltrimethylammonium bromide (CTAB).[13] The conversion yield of this reaction was only 78%, and the final products also contained lots of rods, cubes, tetrahedra, and disks. Shortly after, Sun and coworkers reported the synthesis of Ag nanoplates having sharp tips and edge length of 50−100 nm, together with a conversion yield of

Received: April 16, 2013
Accepted: June 3, 2013
Published: June 3, 2013

   dx.doi.org/10.1021/am401374x | ACS Appl. Mater. Interfaces 2013, 5, 6333−6345

>95%. Specifically, they used the reduction of $AgNO_3$ by $NaBH_4$ in the presence of poly(vinyl pyrrolidone) (PVP) and sodium citrate to initially produce Ag nanoparticles with diameters of ~3.5 nm, followed by refluxing under ambient pressure to form nanoplates in 10 h.[14] In this study, the mechanism was not discussed in detail. Recently, Yin and coworkers demonstrated that the introduction of hydrogen peroxide (H_2O_2) could shorten the reduction of $AgNO_3$ by $NaBH_4$ in the presence of PVP and sodium citrate from hours to minutes with the assistance of various capping ligands containing carboxyl group.[15] Their investigation indicates that H_2O_2 plays an essential role in converting Ag nanoparticles to nanoplates with edge length of 50−100 nm in high yields (close to 100% in the presence of an appropriate capping ligand).

In most of the reported protocols, citrate has been extensively used to induce the formation of Ag nanoplates. Mirkin and coworkers claimed that citrate ions not only served as reducing agents to reduce Ag^+ to Ag^0 in the presence of light irradiation but also helped form plate-structured Ag nanoparticles.[6] They also found that citrate could not be replaced by other carboxyl compounds, such as tricarballylate, citramalate, and aconitate. In the thermal reduction reaction, citrate was mixed with a Ag precursor before the reducing agent was introduced. It is widely accepted that citrate can act as a capping agent to selectively bind to the {111} facets and ultimately promote the selective growth along the lateral direction.[16,17] Much effort has been devoted to understanding the specific role played by citrate ions, but it remains a mystery. It is often referred to as a "magic" reagent. The lack of a comprehensive understanding has limited the research community to repeat most of the reported syntheses in maximum yield and quality because any minor unintentional alteration to the reaction conditions could easily disturb the formation of nanoplates.

Liz-Marzan and coworkers were the first to report "citrate-free" synthesis of Ag nanoplates that relied on the use of N,N-dimethylformamide (DMF) as both a solvent and a reducing agent in the presence of PVP.[18,19] When the concentration of Ag^+ ions was increased relative to the concentration of PVP, nanoplates with edge length of 60−100 nm were observed at 156 °C within 20 min. Unfortunately, the fast reduction at an elevated temperature also led to the formation of Ag nanoplates with a broad size distribution and abundant Ag nanospheres in the final products. Later, Jiang and coworkers used a similar approach to prepare Ag nanoplates of less than 100 nm in edge length in DMF in the presence of PVP through an ultrasound-assisted Ostwald ripening process.[20] In another approach, Xia and coworkers reported the reduction of $AgNO_3$ by PVP in aqueous solutions at 60 °C with no addition of citrate.[21] Their success relied on the use of a weak reducing agent to substantially mitigate the reduction rate and ultimately generate a large proportion of seeds with a plate-like structure for further growth into nanoplates. By controlling the reaction time, nanoplates with edge length between 50−350 nm were obtained but with abundant multiple twinned particles (MPTs) as a byproduct. Most recently, Choi and coworkers reported a similar reduction in *N*-methylpyrrolidone.[22] In most of the published citrate-free reactions, it was indeed very difficult to completely avoid the thermodynamically favored pathway that typically led to the formation of MTPs in the final product. Without removing the MTPs by centrifugation or other means, the nanoplates could constantly grow at the expense of MTPs in a colloidal suspension via O_2-mediated Ostwald ripening under ambient conditions.[23] The variations in size and morphology could lead to constant changes to the optical properties of nanoplates. Hence, there is still a strong need to identify new "citrate-free" approaches with a capability to retain the shape stability and ultimately stabilize their optical properties.

In this article, we demonstrated the synthesis of Ag nanoplates with edge length of 50 nm in high conversion yield (>99%) and reproducibility using a citrate-free solvothermal route where the precursor, reductant, and solvent are placed in a sealed pressured vessel and heated to a temperature slightly above the boiling point of the solvent.[24,25] Specifically, when $AgNO_3$ was reduced by PVP in ethanol under a solvothermal condition, Ag MTPs were quickly formed to drastically reduce the concentration of Ag^+ ions in the solution, activating the formation of plate-like seeds through a kinetically controlled route. When the mixture of MTPs and plate-like seeds was subjected to a solvothermal condition, Ostwald ripening would occur between these two species, leading to the growth of plate-like seeds into small nanoplates and then larger nanoplates at the expense of the MTPs. With the assistance of O_2, the Ostwald ripening process could be accelerated to enable a complete conversion of the Ag MTPs into nanoplates in a few hours. Previously, a few research groups have documented solvothermal syntheses of Ag nanoparticles with different shapes that include wires, cubes, spheres, rods, and plates.[26−28] However, our work represents the first successful attempt to reproducibly generate uniform Ag nanoplates in >99% conversion yield using the simple reduction of $AgNO_3$ by PVP in ethanol under solvothermal condition. Whereas Liz-Marzan[18] and Xia[21] previously reported a similar reduction route under ambient conditions, our approach embraces a unique capacity to generate Ag nanoplates with no concomitance of Ag MPTs. This work further demonstrates that citrate is, perhaps, not necessary at all in the formation of Ag nanoplates. In fact, the exclusion of citrate not only improves the reproducibility of the synthesis but also gives the Ag nanoplates excellent stability. Furthermore, we confirmed that the solvothermal condition could be used to significantly shorten the reaction time when compared with reactions that were conducted by refluxing under ambient pressure. The formation of a larger number of plate-like seeds under a solvothermal condition also made it possible to reduce the lateral dimensions of the nanoplates to ~50 nm. All of these unique attributes embrace promises to further develop the solvothermal reaction as an effective route to the production of various types of nanomaterials.

2. EXPERIMENTAL SECTION

Chemicals. Silver nitrate ($AgNO_3$, 99+%), silver trifluoroacetate (CF_3COOAg, >99.99+%), poly(vinyl pyrrolidone) with molecular weights of 10000, 29000, 55000 (PVP-10K, PVP-29K, and PVP-55K), and ethanol (200 proof) were all purchased from sigma-Aldrich and used as received.

Synthesis of Ag Nanoplates. The Ag nanoplates were prepared by heating a mixture of $AgNO_3$ and PVP in ethanol to 80 °C in acid digestion vessels (Parr Instrument Company, vessel number 4745). In a standard procedure, $AgNO_3$ and PVP-29K were separately dissolved in ethanol at concentrations of 10.0 and 1.0 mM (in terms of the molecular weight of PVP), respectively. Next, 10 mL of the as-prepared PVP solution was added into a Teflon liner, followed by the addition of 0.3 mL of the $AgNO_3$ solution. The Teflon liner was then sealed, placed in the stainless vessel, and heated in an oven at 80 °C for 4 h. Upon completion, the vessel was water cooled to room

Table 1. Summary of Reaction Conditions

Experiment	Standard Condition	Variation
Typical Synthesis (Fig. 1 and 2)	10 mL 1 mM PVP29K 0.3 mL 10 mM $AgNO_3$ At 80 °C	Reaction time: 0.5, 1, 1.5, 2, 2.5, 3, 3.5, 4 hours
Role of [PVP]/[$AgNO_3$] (Fig. 4)	10 mL PVP29K 10 mM $AgNO_3$ At 80 °C for 4 hours	PVP concentration and $AgNO_3$ volume: Fig. 4 A B C D E F PVP (mM) 1 2 1 0.5 2 0.5 $AgNO_3$(mL) 0.15 0.3 0.6 0.3 0.6 0.15
Role of [PVP]/[$AgNO_3$] (Fig. 5)	At 80 °C for 4 hours	PVP and $AgNO_3$ concentrations Fig. 5 A B C PVP 10mL 1 mM 2 mL 4 mM $AgNO_3$ 0.9 mL 10 mM Product of Fig. 5 A (mL) 4 mL 4 mL
Role of Ethanol (Fig. 6)	10 mL 1 mM PVP29K 0.3 mL 10 mM $AgNO_3$ At 80 °C for 4 hours	The volume of DI water: 0.01, 0.05, 0.1, 0.2, 0.5, 1 mL
Role of Reaction Volume (Fig. 7)	10 mL 1 mM PVP29K 0.3 mL 10 mM $AgNO_3$ At 80 °C for 4 hours	The volume of reaction solution: 5, 15, 20 mL
Role of Reaction Temperature (Fig. 9)	10 mL 1 mM PVP29K 0.3 mL 10 mM $AgNO_3$	Reaction temperature and time: 160 °C (1hour) 60 °C (21hours) Room temperature (40 days)
Overgrowth (Fig. 10)	10 mL 1 mM PVP29K 0.3 mL 10 mM $AgNO_3$ At 80 °C	Reaction time: 4, 6, 7, 8, 9, 24 hours
Seed-mediated Growth (Fig. 11)	1 mL original product of a typical synthesis 10 mL 1 mM PVP29K 0.3 mL 10 mM $AgNO_3$ At 80 °C	Reaction time: 1, 2, 2.5, 3, 4 hours

temperature prior to disassembly. To characterize the sample, 1.5 mL of the as-prepared solution was used to record UV−vis spectra, followed by centrifugation at a speed of 150,000 rpm to separate the solid and supernatant into two samples for Ag content measurements by inductively coupled plasma mass spectrometry (ICP-MS). For the preparation of TEM samples, the nanoparticles were collected by centrifugation at a speed of 15,000 rpm, washed three times with ethanol to remove access PVP, re-dispersed in ethanol, dropped on TEM grids, and then dried under ambient conditions.

Instrumentation and Characterization. Transmission electron microscopy (TEM) images were taken using a JEM-1400 microscope (JEOL, Tokyo, Japan) operated at 120 kV. High resolution TEM images were captured using a JEOL 4000EX microscope (JEOL, Tokyo, Japan) operated at 400 kV. The UV−vis spectra were recorded using a Cary 50 UV−vis spectrometer (Agilent Technologies, Santa Clara, CA). The measurements of Ag contents were performed using an inductively coupled plasma mass spectrometer (NexION 300Q, Perkin-Elmer). A routine centrifuge (Eppendorf 5430) and high-speed centrifuge (Max-XP Ultracentrifuge, Beckman Coulter Optima) were used, respectively, for the collection/washing of particles and preparation of ICP-MS samples.

3. RESULTS AND DISCUSSION

In a typical synthesis of Ag nanoplates, PVP of different molecular weights was mixed with $AgNO_3$ and ethanol in a Teflon liner, followed by a solvothermal process in a stainless vessel at 80 °C for 4 h. We have conducted experiments under different combinations of reaction conditions to elucidate the roles played by various parameters in affecting the formation of Ag nanoplates. For example, we carried out syntheses by systematically varying the concentrations of $AgNO_3$ and PVP, reaction time, and temperature/pressure. In additional to the experimental details described in each subsection of the Results and Discussion, a full list of experimental conditions is available in Table 1.

Quantitative Analysis of Solvothermal Reaction. We used UV−vis spectroscopy to characterize the products that were obtained by quenching the reaction of a standard synthesis at different time points. To gain a quantitative understanding of the reduction of Ag^+ ions, we also used ICP-MS to measure the contents of Ag in the product solution and supernatant (unreduced Ag^+ ions), respectively, of each synthesis after supernatant had been collected by high-speed centrifugation to remove nanoparticles. Figure 1 shows the UV−vis spectra and ICP-MS data, respectively, of the products obtained at various reaction times up to 4 h. As limited by the solvothermal vessels we used, we were unable to follow the early nucleation and growth events within the initial 0.5 h of a synthesis. However, we could still identify all the major features involved in the formation of Ag nanoplates, including the MTPs, the plate-like seeds, and the conversion between these two species. At 0.5 h, we observed one strong peak centered at 400 nm in the UV−vis spectrum, which suggests the formation of nanoparticles with a more or less isotropic shape and relatively small size in the early stage of the reaction.[9] The ICP-MS result indicates that more than 90% of the initially added Ag^+ ions had been reduced into Ag atoms, which then nucleated and grew into the nanoparticles, leading to a significant decrease in Ag^+ concentration from 291 to 27 μM in the reaction solution. As the reaction progressed, the peak at

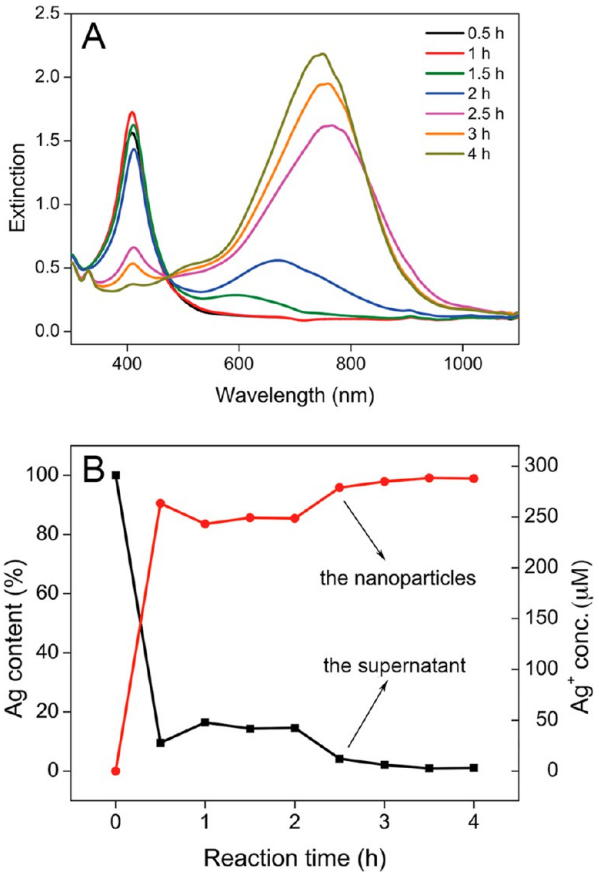

Figure 1. (A) UV−vis spectra of Ag nanoparticles obtained from eight standard syntheses quenched at different reaction times. (B) ICP-MS data of the corresponding products (solids and supernatants) showing the percentages of initially added $AgNO_3$ that had been converted into Ag nanoparticles (solids) and that remained in the reaction solutions (supernatants). Ag^+ concentration only applies to the supernatant.

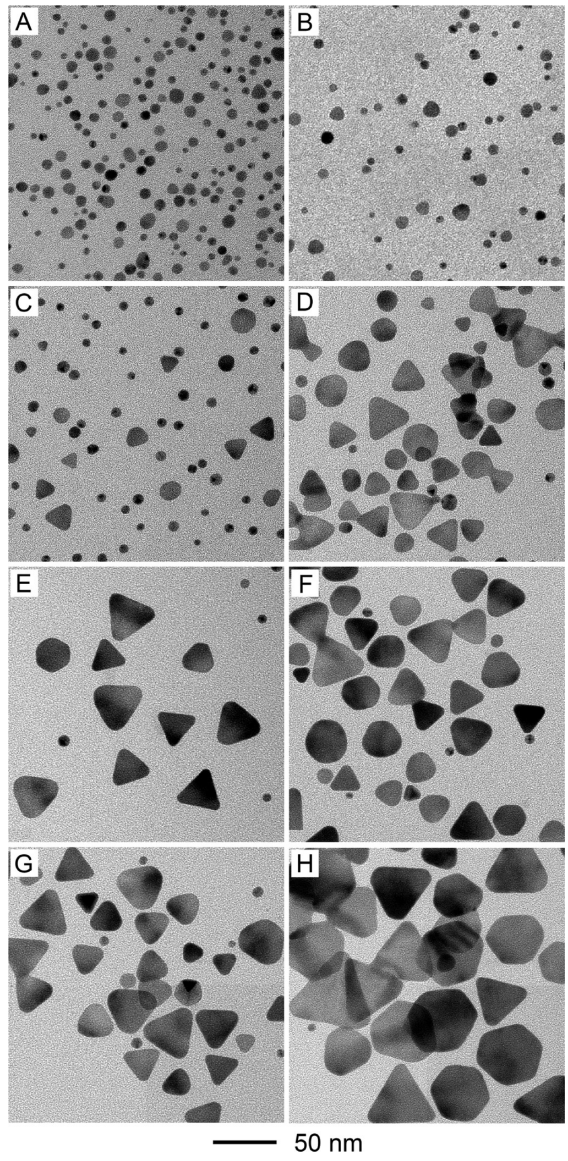

Figure 2. TEM images of Ag nanoparticles obtained from eight standard syntheses stopped at different reaction times: (A) 0.5, (B) 1, (C) 1.5, (D) 2, (E) 2.5, (F) 3, (G) 3.5, and (H) 4 h. These images were taken from the same samples shown in Figure 1.

400 nm slightly increased in intensity, followed by a quick drop with concomitant growth of two new peaks at 750 and 330 nm, which can be assigned to the in-plane dipole and out-of-plan quadrupole resonances of Ag nanoplates, respectively.[4] The existence of an isosbestic point at 460 nm in the UV−vis spectra suggests a direct transformation process that involved the consumption of Ag spherical nanoparticles and simultaneous growth of Ag nanoplates. The ICP-MS data indicate that the Ag^+ concentration was maintained at a more or less stable level of 44 μM from 1.0 to 2.0 h, during which the spherical nanoparticles started to be etched although they were still in dominance. Once the transformation from spherical nanoparticles to nanoplates was accelerated, the Ag^+ concentration was quickly reduced to 12 μM (t = 2.5 h) and finally to 2.8 μM (t = 4.0 h). At the end, the UV−vis spectrum shows essential disappearance of the peak at 400 nm and a strong peak at 750 nm. As confirmed by the ICP-MS data, >99% of the originally added Ag^+ ions had been converted into the Ag nanoplates by this point.

The UV−vis and ICP-MS results are consistent with our TEM observations. Figure 2 shows TEM images of the corresponding solid products that were obtained at different reaction times. Figure 2A and B shows the formation of Ag nanoparticles with a more or less spherical shape in the early stage. The high-resolution TEM images in Figure S1 of the Supporting Information indicate that these nanoparticles had an average size less than 10 nm, and most of them were MTPs. A small portion of the particles had a plate-like structure with stacking faults along the vertical direction.[29] The samples in Figure 2C and D correspond to the initial stage of transformation, during which Ag nanoplates began to grow at the expense of Ag MTPs. As shown in Figure 2E−H, the population of Ag nanoplates increased with reaction time whereas that of MTPs decreased. At the end, Ag nanoplates with snipped corners were formed. Their average thickness and edge length were 6.4 ± 0.7 and 50.0 ± 7.4 nm, respectively.

Mechanistic Insight. From the UV−vis, ICP-MS, and TEM data, we can begin a mechanistic understanding of the effective conversion from Ag^+ ions to Ag nanoplates in our solvothermal synthesis. Figure 3 outlines a schematic of the proposed mechanism that includes (i) fast reduction of Ag^+ ions to generate Ag MTPs and at the same time depletion of most of the Ag^+ ions in the solution, (ii) formation of plate-like seeds under a kinetically controlled condition due to the low

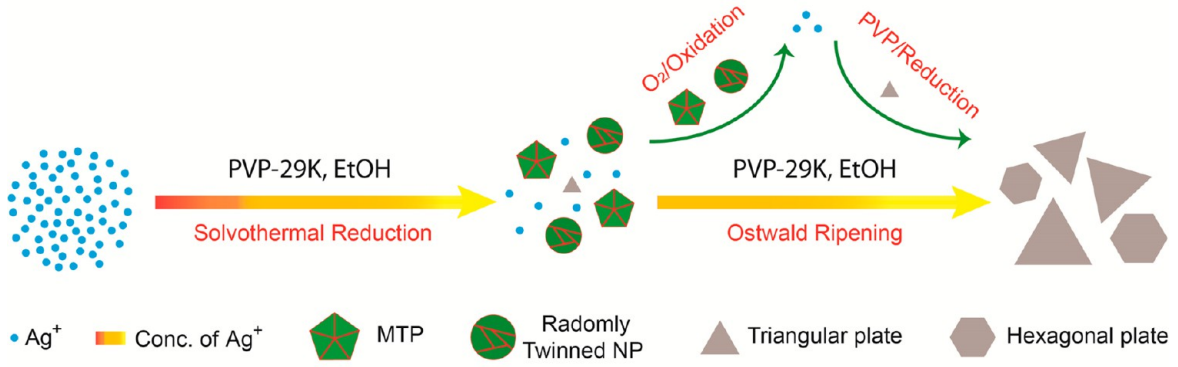

Figure 3. Schematic diagram of the mechanism proposed to account for the formation of Ag nanoplates with a conversion yield approaching 100%. This mechanism involved the formation of twinned nanoparticles and plate-like seeds in the early stage, followed by the growth of the seeds into larger nanoplates at the expense of nanoparticles in the late stage.

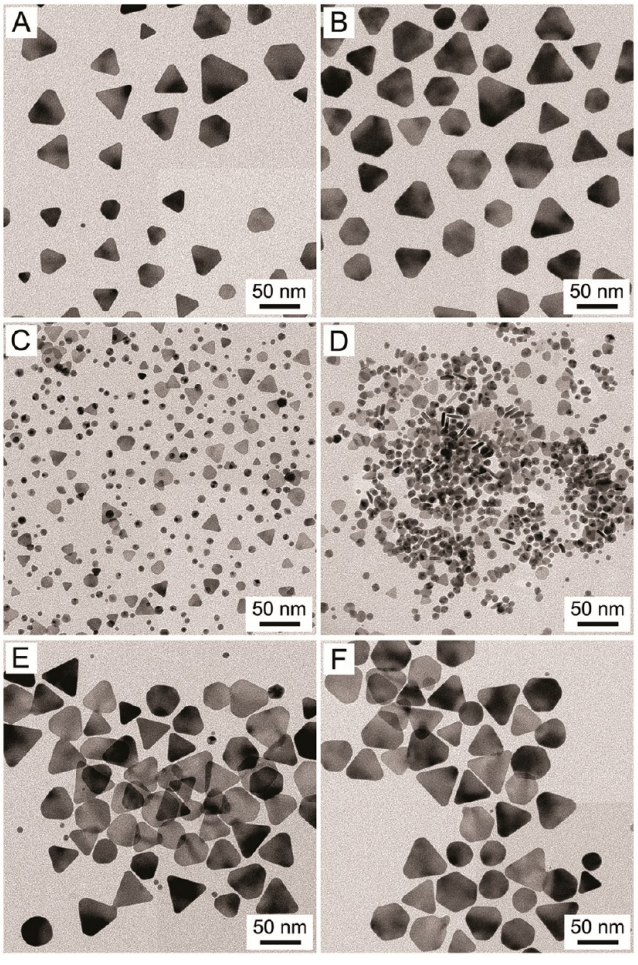

Figure 4. TEM images of Ag nanoparticles prepared using the standard procedure except that the PVP/$AgNO_3$ molar ratio was varied: (A, B) increase in the PVP/$AgNO_3$ molar ratio to 20:3; (C, D) decrease in the PVP/$AgNO_3$ molar ratio to 5:3; and (E, F) increase in the PVP/$AgNO_3$ molar ratio in (C, D) to 10:3.

concentration of Ag^+ ions in the solution, followed by their further growth into small nanoplates, and (iii) oxidative etching to initiate and then facilitate the transformation from Ag MTPs to larger nanoplates via an Ostwald ripening process.

In the solvothermal reaction, the reduction of Ag^+ ions by PVP and ethanol was a thermodynamically controlled process in which Ag atoms were supposed to nucleate and grow into MTPs to attain minimal total surface energy.[8] Our results indicate that both PVP and ethanol could serve as reducing agents to promote the formation of MTPs with sizes smaller than 10 nm and in a high conversion yield (>90%). The quick consumption of most Ag^+ ions during the formation of MTPs effectively reduced their concentration to a level of 27 μM at t = 0.5 h, and consequently, the reduction became much slower, favoring kinetically controlled formation of the plate-like seeds with stacking faults. As the reaction progressed, the plate-like seeds were able to grow into larger sizes, whereas the MTPs were confined to a relatively constant size less than 10 nm without further growth. Once the concentration of Ag^+ ions was depleted to an extremely low concentration, the MTPs with sizes less than 10 nm as well as twin boundary defects became susceptible to the O_2 trapped in the reaction vessel.[30,31] In an Ostwald ripening process, the MTPs were constantly attacked by the O_2, oxidized, and dissolved into the solution, followed by the reduction of these dissolved Ag^+ by PVP and ethanol to generate fresh Ag atoms that were then added onto the nanoplates to enlarge their lateral dimensions.[32,33] Our ICP-MS results show that the concentration of Ag^+ ions remained at an extremely low concentration (< 12 μM) during the conversion from Ag MTPs to nanoplates. As indicated by the isosbestic point in the UV−vis spectra, the Ag atoms dissolved from the MTPs were reduced and deposited onto nanoplates via seeded growth without involving additional self-nucleation and growth. To further support this proposed mechanism, we examined many other conditions, including the type of silver precursor, molecular weight of PVP, molar ratio of PVP to $AgNO_3$, role of ethanol, and involvement of O_2, as well as the effects of pressure and temperature.

Effects of $AgNO_3$ and PVP. Silver nitrate is a good choice of Ag precursor in the direct chemical reduction of Ag^+ ions to form Ag nanoparticles by refluxing under ambient pressure.[34] In this case, it is possible to generate a small amount of HNO_3 that could serve as an oxidative etchant to help dissolve the MTPs.[35] To exclude the possible role of HNO_3, we replaced the $AgNO_3$ with CF_3COOAg in a standard synthesis while all other conditions were preserved. As shown in Figure S2 of the Supporting Information, we obtained Ag nanoplates that were essentially identical to those prepared using $AgNO_3$. This result indicates that HNO_3 only had a minor impact, if any, on the formation of Ag MTPs and plate-like seeds in our synthesis, as well as the transformation from MTPs to nanoplates.

dx.doi.org/10.1021/am401374x | ACS Appl. Mater. Interfaces 2013, 5, 6333−6345

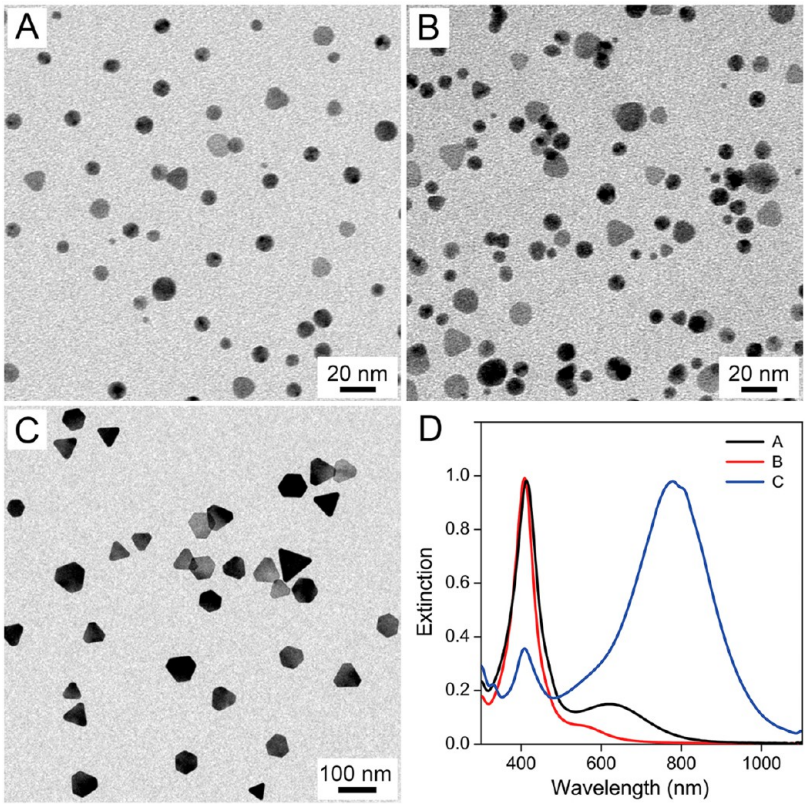

Figure 5. TEM images of Ag nanoparticles (A) prepared using the standard procedure except for the use of 0.9 mL $AgNO_3$ and (B, C) obtained from a second-round solvothermal treatment of the as-prepared sample shown in (A) without or with the addition of 2.0 mL 4.0 mM PVP-29K, respectively. (D) Corresponding UV−vis spectra for the samples shown in (A−C).

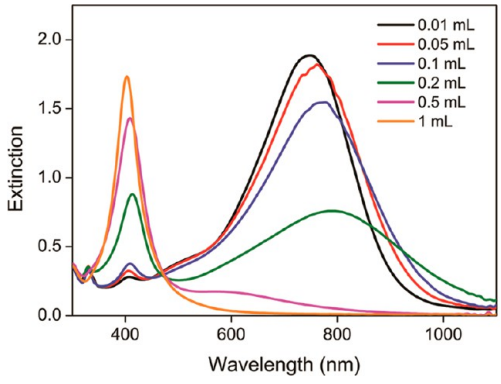

Figure 6. UV−vis spectra of the samples prepared using the standard procedure except that different volumes (marked on the curves) of DI water were added before solvothermal treatment.

PVP is widely used in the chemical synthesis of colloidal nanocrystals with its roles being documented as a steric stabilizer or capping agent.[36] Xia and coworkers also demonstrated that the hydroxyl end groups of PVP had a mild reducing power to reduce $AgNO_3$ into elemental Ag in an aqueous solution at 60 °C. The reduction was sufficiently slow that the growth of Ag nanocrystals became kinetically controlled, leading to the formation of Ag nanoplates with edge lengths around 400 nm.[21,37] Later, Liz-Marzan and coworkers reported that PVP manipulated the reduction rate of Ag^+ to Ag^0 by forming a complex with Ag^+ ions, followed by the reduction of this complex by PVP.[38,39] They also reported that Ag^+ ions could be reduced by ethanol when certain surfactants were present. Most recently, the reduction kinetics of $AgNO_3$ by PVP in ethanol under ambient pressure was further studied by several groups for the formation of Ag nanoparticles, and it was found that the reduction rate constant depended strongly on the ratio of PVP to $AgNO_3$ and reaction temperature.[40] However, none of these studies systematically investigated the reduction kinetics of $AgNO_3$ by PVP in ethanol under a solvothermal condition, not mentioning its use for the synthesis of Ag nanoplates.

As shown in Figure 2H for the standard synthesis, we obtained Ag nanoplates with an edge length of 50 nm when the corresponding molar ratio of PVP to $AgNO_3$, [PVP]/[$AgNO_3$], was set to 10:3. To elucidate the specific role of PVP in the solvothermal reduction of $AgNO_3$ in ethanol, we finely tuned the reduction rate by varying the molar ratio of PVP-29K to $AgNO_3$ and thereby evaluate its impact on the formation of Ag nanoplates. In the first set of experiments, we prepared reaction solutions with [PVP]/[$AgNO_3$] other than 10:3 by either changing the volume of the $AgNO_3$ solution or varying the concentrations of PVP-29K. For example, we performed two reactions at [PVP]/[$AgNO_3$] = 20:3 by either reducing the volume of $AgNO_3$ from 0.3 mL to 0.15 mL or doubling the concentration of PVP-29K to 2.0 mM, respectively. Figure 4A and B shows TEM images of samples obtained under these two conditions, both of them contained Ag nanoplates of 50 nm in edge length. In contrast, when we changed [PVP]/[$AgNO_3$] to 5:3 by either doubling the volume of $AgNO_3$ to 0.6 mL or reducing the concentration of PVP-29K to 0.5 mM, respectively, we obtained mixtures of MTPs, plates, and irregular nanoparticles, as shown in Figure 4C and D. It is evident that a shortage of PVP in the reaction solution was unable to sustain the Ostwald ripening process, leading to the

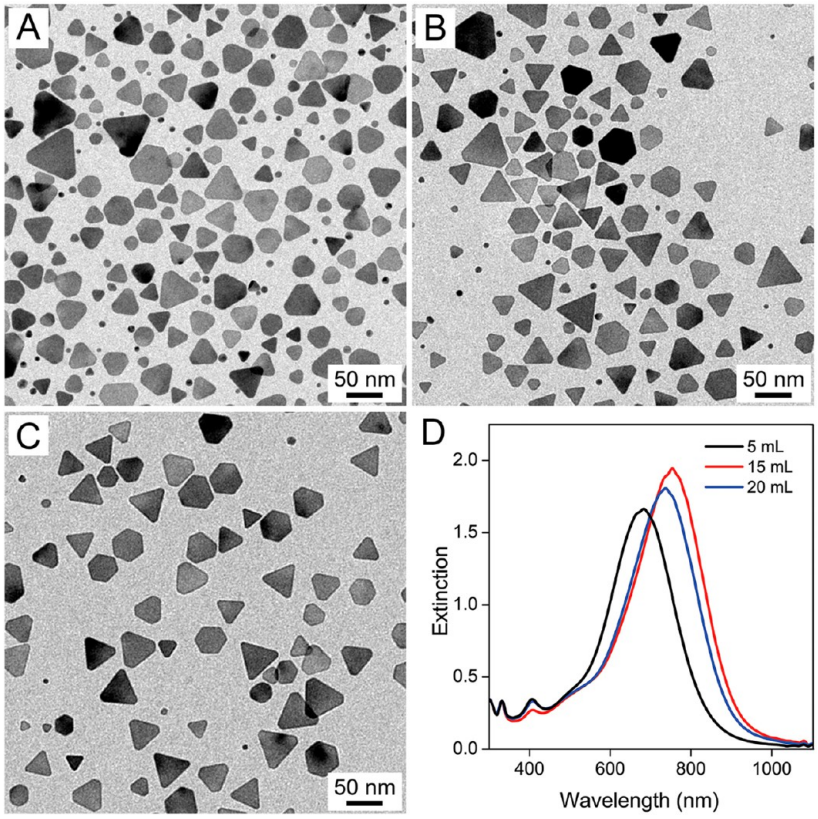

Figure 7. TEM images of Ag nanoparticles prepared using the standard procedure except for the use of reaction solution at different volumes: (A) 5, (B) 15, and (C) 20 mL. (D) Corresponding UV−vis spectra of these samples.

formation of Ag MTPs in the final products with an incomplete conversion from MTPs to nanoplates.

When we increased [PVP]/[$AgNO_3$] from 5:3 to 10:3 by either increasing the concentration of PVP or reducing the volume of $AgNO_3$, Ag nanoplates were formed again. Figure 4E and F shows TEM images of Ag nanoplates that were obtained under the following two conditions: PVP-29K (2.0 mM, 10 mL) and $AgNO_3$ (10 mM, 0.6 mL) or PVP-29K (0.5 mM, 10 mL) and $AgNO_3$ (10 mM, 0.15 mL). Figure S3 of the Supporting Information shows the corresponding UV−vis spectra taken from the final products. Combined together, these results indicate that Ag nanoplates with an edge length of 50 nm could be formed all the time when [PVP]/[$AgNO_3$] was greater than 10:3. It is obvious that PVP in ethanol plays an essential role in controlling the reduction rate that drives the formation of MTPs from $AgNO_3$ in the early stage of a synthesis and promotes the transformation from Ag MTPs to nanoplates in the late stage.

It is worth noting that the edge length of nanoplates and their corresponding LSPR resonance peak positions cannot be tuned by varying the concentration of $AgNO_3$. For example, Figure S3A of the Supporting Information shows UV−vis spectra of two batches of Ag nanoplates that were prepared with $AgNO_3$ at concentrations of 148 and 566 μM, respectively. We found that the in-plane dipole resonance peak at 750 nm was unchanged, although the peak intensity showed a strong dependence on the concentration of $AgNO_3$—the more $AgNO_3$ was used, the more Ag nanoplates with the same edge length (50 nm) would be formed. These observations suggest that the concentration of $AgNO_3$ had an influence on the reduction rate and ultimately the population and size of MTPs formed in the early stage, but the edge length of the Ag nanoplates was likely determined by the ratio between the total amount of $AgNO_3$ added into the solution and the number of plate-like seeds formed.

To further support our mechanism, we performed a new synthesis at [PVP]/[$AgNO_3$] = 10:9 by using 10 mL of 1.0 mM PVP-29K and 0.9 mL of 10 mM $AgNO_3$. After solvothermal reduction at 80 °C for 4 h, Ag MTPs and some nanoplates were formed in the solution (Figure 5A). We took 4 mL of this as-prepared solution and subjected it to another 4 h of solvothermal treatment. As shown in Figure 5B, the nanoparticles were found to retain similar distributions in terms of both size and shape; there was no conversion from MTPs to nanoplates. However, when we introduced additional PVP-29K (4.0 mM, 2 mL) into the other 4 mL of the as-prepared solution prior to the second round of solvothermal reduction for 4 h, Ag nanoplates were formed at the expense of MTPs in the system (Figure 5C). Figure 5D shows the corresponding UV−vis spectra of these three different products, from which we evidently identify the essential role of PVP-29K in facilitating the conversion from Ag MTPs to nanoplates.

We also evaluated the significance of the molecular weight of PVP in the synthesis. Previous work has demonstrated that the reducing power of PVP increased as the molecular weight of PVP was decreased.[21] This may affect the formation MTPs and plate-like seeds in the initial stage, as well as the transformation from MTPs to nanoplates in the late stage. To understand the effect of molecular weight on the formation Ag nanoplates, we performed two reactions at 80 °C for 4 h with [PVP]/[$AgNO_3$] = 10:3 by using PVP-10K and PVP-55K, respectively. Figure S4 of the Supporting Information shows TEM images and the

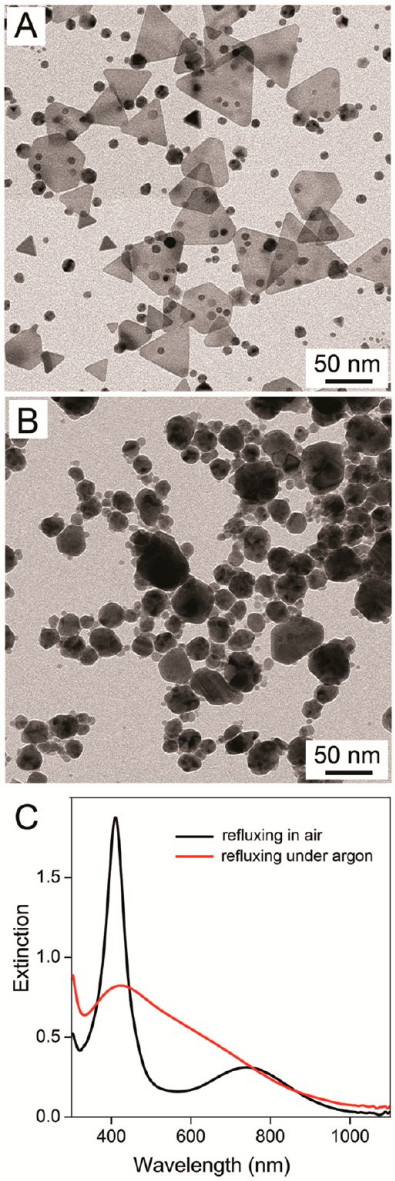

Figure 8. TEM images of nanoparticles obtained from a standard synthesis that was carried out under refluxing in the presence of (A) air and (B) argon, respectively. (C) Corresponding UV–vis spectra of these two samples.

corresponding UV–vis spectra of the solid products. In the case of PVP-10K, the increased reducing power led to the formation of a larger population of small MTPs and a smaller number of plate-like seeds in the early stage and thus larger nanoplates in the final product. Becaue of the smaller number of plate-like seeds, the transformation from Ag MTPs to nanoplates was incomplete. Alternatively, the weaker reducing power of PVP-55K resulted in the formation of MTPs and small plates because the Ostwald ripening process was retarded. This result was consistent with the previous observation when inadequate PVP was added into the reaction system. Taken together, these results reiterate the critical role of PVP-29K with the appropriate reduction kinetics to promote the formation of plate-like seeds in the early stage of a synthesis and ensure a high efficiency for the conversion from Ag MTPs to nanoplates in the late stage.

Role of Solvent. To elucidate the role of ethanol, we performed three control reactions at 80 °C for 4 h by adding 0.3 mL of the 10 mM $AgNO_3$ solution (either in ethanol or DI) into the following solutions: 10 mL ethanol, 10 mL DI water, and 10 mL DI water containing 1.0 mM PVP29K, respectively. Figure S5A of the Supporting Information shows UV–vis spectra of the as-prepared products, with no formation of Ag nanoplates in any of these systems. This result suggests that the reduction rate of $AgNO_3$ in ethanol was increased considerably with the introduction of PVP-29K. In fact, we noticed the occurrence of yellowish color shortly after we mixed $AgNO_3$ with PVP-29K in ethanol at room temperature in the absence or presence of light. The reduction led to the formation of Ag nanoparticles with LSPR peak at 400 nm after 5 h under the ambient condition, whereas the same reaction in ethanol alone showed no formation of nanoparticles (Figure S5B, Supporting Information). These results demonstrate that a combination of PVP-29K and ethanol offers a unique approach to manipulating the reduction rate of $AgNO_3$ under solvothermal condition to produce Ag nanoplates in high yields.

To further understand the role of ethanol, we performed a series of reactions by introducing various amounts of DI water into the reaction solution based on ethanol. Figure 6 shows UV–vis spectra of the products that were prepared using the standard procedure with 10.3 mL total volume of ethanol reaction solution at 80 °C for 4 h. Evidently, the added DI water mitigated the reduction rate of $AgNO_3$ and ultimately the conversion efficiency from Ag MPTs to nanoplates. For example, when we increased the volume of DI water to 0.2 mL (~2% of the volume of ethanol), the population of MTPs with an LSPR peak at 400 nm increased with a decrease for the nanoplates with an LSPR peak at 750 nm. With a further increase in DI water to 0.5 mL (~5%), the reduction rate was substantially reduced, leading to the formation of Ag MTPs in the final product. At 1 mL DI in the reaction solution of ethanol (~9%), the product only contained MTPs.

Role of O_2. In our proposed mechanism, O_2 plays an essential role in promoting the effective transformation from Ag MTPs to nanoplates through oxidative etching. It can also affect the reduction kinetics in the early stage of a synthesis and thus the formation of both MTPs and plate-like seeds. In the standard synthesis, 10 mL of the solution was sealed in a 23 mL Teflon liner. As a result, 13 mL (or 5.3×10^{-4} mol based on the ideal gas law calculation) of air—a mixture of 21% O_2 and 79% N_2— was trapped in the reaction container at 25 °C. Under the solvothermal condition at 80 °C, the air should be completely mixed with the ethanol steam and the total amount of O_2 available for the oxidative etching process was 1.1×10^{-4} mol. The total amount of Ag atoms involved in the synthesis was 3×10^{-6} mol. As a result, the amount of O_2 in the ethanol steam was in excess as compared to the Ag atoms in the MTPs that had to be oxidized during the Ostwald ripening process.

To validate our hypothesis about the role of O_2, we modified the standard procedure by using different volumes of reaction solution while keeping all other reactions parameters unchanged. Figure 7 shows TEM images and the corresponding UV–vis spectra of three products obtained at 80 °C for 4 h by using reaction solutions at 5, 15, and 20 mL, respectively. Ag nanoplates were formed in all these syntheses. These results suggest that the amounts of O_2 in all these syntheses were sufficient to completely oxidize all Ag MTPs and thus ensure their complete transformation into nanoplates. For the synthesis with 5 mL solution, an increased amount of O_2 in

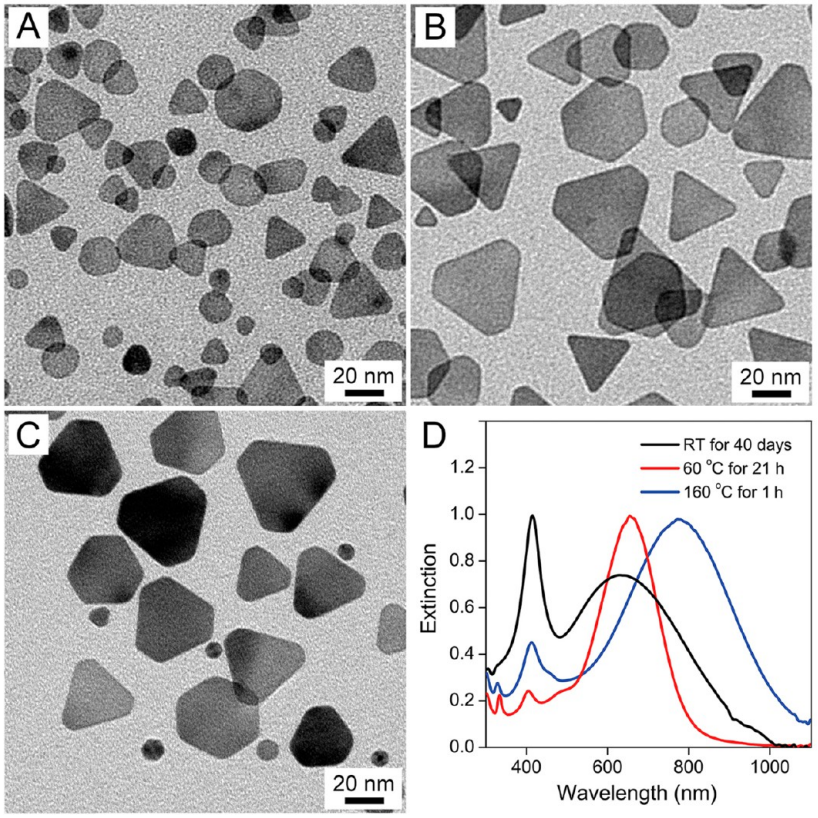

Figure 9. TEM images of the Ag nanoparticles that were prepared using the standard procedure except for the reaction temperature and time: (A) at room temperature for 40 days, (B) at 60 °C for 21 h, and (C) at 160 °C for 1 h, respectively. (D) Corresponding UV−vis spectra.

the ethanol steam led to corner truncation for the Ag nanoplates and thus a blue-shifted LSPR peak centered at 700 nm. The truncation of corners was so significant that the resultant Ag^+ ions could be further reduced to induce self-nucleation and growth, generating the small MTPs and nanoplates shown in the final product. These small MTPs and nanoplates were responsible for the weak peak at 400 nm and shoulder peak at 500 nm, respectively. As for the sample prepared with 15 or 20 mL of solution, a decreased amount of O_2 in the ethanol seems to have no impact on the formation of Ag nanoplates and their LSPR peak positions when compared with those of 10 mL solution (Figures 1A and 2H).

We also performed a control experiment under argon (Ar) protection. Because of the complication in replacing all air with Ar in a solvothermal system, we conducted the synthesis under refluxing with a condensation system. Figure 8 shows TEM images and the corresponding UV−vis spectra of the products obtained at 80 °C with and without Ar protection, respectively. When O_2 was absent, MTPs and aggregated particles were formed with a broad and uncharacteristic LSPR peak. In contrast, Ag nanoplates with an edge length of 50 nm were observed in the presence of O_2, while the product also contained MTPs (with an LSPR at 400 nm) and smaller plates (with an LSPR at 750 nm). This observation demonstrates the important role of O_2 in the oxidative etching of MTPs for their conversion into Ag nanoplates via an Ostwald ripening process.

Effect of Reaction Temperature. Temperature could affect the reduction kinetics of Ag^+ ions, and ultimately the formation of Ag nanoplates in ethanol.[40] It could also induce the effect of pressure due to the use of a solvothermal condition. To understand these effects, we performed solvothermal syntheses using the standard procedure at different temperatures and for different periods of time. Figure 9 shows TEM images and corresponding UV−vis spectra of the samples prepared at room temperature and by the solvothermal reactions at 60 °C, and 160 °C, respectively. The reduction was extremely slow at room temperature, leading to the formation of Ag MTPs and nanoplates after 40 days (Figure 9A). With an increase in reaction temperature to 60 °C under solvothermal condition, Ag nanoplates with an LSPR peak at 650 nm were formed after 21 h (Figure 9B). When the reaction temperature reached 80 °C, a little bit above the boiling point of ethanol at 79 °C, the formation of Ag nanoplates with an LSPR peak at 750 nm was completed after 4 h (Figure 1A). A further increase in reaction temperature to 160 °C allowed for the formation of Ag nanoplates with an LSPR peak at 780 nm after only 1 h (Figure 9C). These results suggest that an increase in temperature could induce quick reduction of $AgNO_3$ to form MTPs in the early stage, as well as a faster Ostwald ripening process in the late stage. The use of a temperature slightly above the boiling point of ethanol allowed us to avoid high pressure in the reaction vessel while generating pure Ag nanoplates within a relatively short period of time around 4 h.

Plasmonic Properties of the Ag Nanoplates. The structural anisotropy of Ag nanoplates embraces unique LSPR properties.[41] It has been reported that the in-plane dipole LSPR peak of a Ag nanoplate red shifts when its edge length was increased or when the corner truncation was reduced.[5] In this work, we developed two strategies for tailoring the structures of Ag nanoplates and thus tune their in-plane dipole LSPR peaks from the visible to the near-infrared region. Unlike many previously reported syntheses where the edge length of the

dx.doi.org/10.1021/am401374x | ACS Appl. Mater. Interfaces 2013, 5, 6333−6345

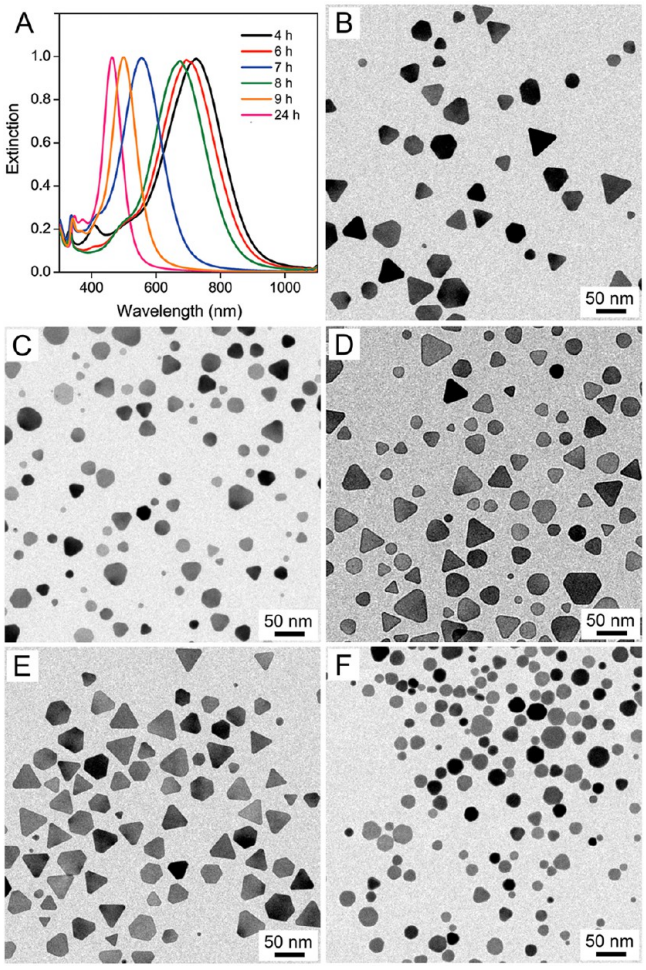

Figure 10. UV–vis spectra and TEM images of Ag nanoplates with tunable optical properties that were obtained by extending the reaction time. (A) UV–vis spectra of the products obtained from standard syntheses where the reaction time was prolonged from 4 h up to 24 h. (B–F) TEM images of the corresponding products obtained at different times: (B) 6, (C) 7, (D) 8, (E) 9, and (F) 24 h.

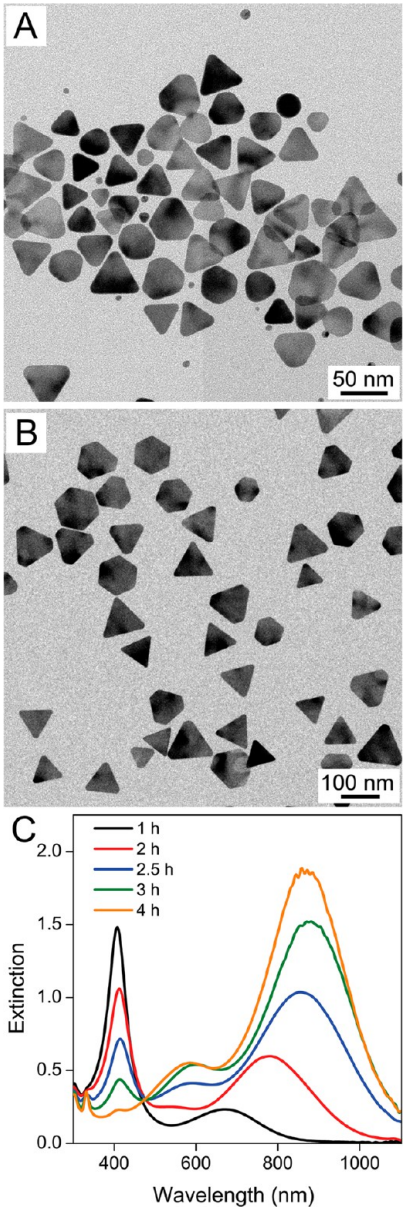

Figure 11. Seed-mediated growth for larger Ag nanoplates with their LSPR peaks being tuned in the near-infrared region. TEM image of (A) Ag nanoplates that served as the seeds and (B) the product obtained from seed-mediated growth at t = 4 h. (C) UV–vis spectra correspond to the products of seed-mediated growth stopped at different reaction time points.

nanoplates was determined by the concentration of Ag precursor, our process relies on the formation of Ag MTPs and their conversion into nanoplates to define the length scale. In our case, an increase in $AgNO_3$ concentration led to the formation of Ag nanoplates with the same edge length but in larger quantities. As a result, we could obtain Ag nanoplates of 50 nm in edge length with LSPR peaks at 750 nm routinely and reproducibly (Figure 1A). One approach to tuning the LSPR resonance to blue was to simply keep the solvothermal reaction over a longer period of time, in which the Ag nanoplates evolved into truncated plates with an increase in snip size.[42] Figure 10A shows UV–vis spectra of the samples obtained at different reaction times. The corresponding TEM images (Figure 10B–F) indicate an interplay of two processes in the course of reaction: the truncation of "old" Ag nanoplates due to oxidation and the formation of "new" Ag nanoplates through additional solvothermal reduction of the dissolved Ag^+ ions by PVP and ethanol. As a result, we could constantly shift the UV–vis spectra of the Ag nanopates from 750 to 460 nm. Additionally, we found that round disks were formed at 80 °C if the reaction was allowed to proceed for 24 h, with the LSPR dipole peak located at 460 nm. This result implies a continuous etching process and the Ag^+ ions released from the sharp corners of the Ag nanoplates undertook reduction and thus promoted another round of growth process to form new plates. Together, these two processes led to the formation of rounded plates (disks) at the end.[43,44]

Alternatively, we could tune the LSPR peaks of the Ag nanoplates to the near-infrared by increasing the edge length through seed-mediated growth under solvothermal condition by using the as-prepared Ag nanoplates of 50 nm in edge length as the seeds.[45] Figure 11A shows TEM image of Ag nanoplates formed using the standard solvothermal process that involved the reduction of $AgNO_3$ by PVP-29K in ethanol at a molar ratio of 10:3 at 80 °C for 4 h. We then used 1 mL of the Ag nanoplates as seeds to mix with $AgNO_3$ (10.0 mM, 0.3 mL) and PVP-29K (1.0 mM, 10 mL) in ethanol. In this case, the newly

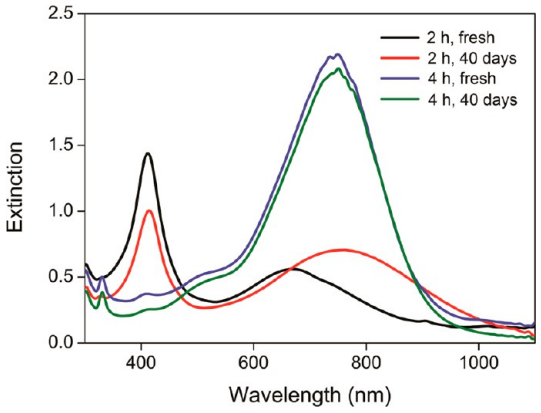

Figure 12. UV−vis spectra of the samples that were obtained by stopping standard syntheses at 2 and 4 h, respectively. Samples were then left in capped vials without disturbance for 40 days.

added $AgNO_3$ would be reduced to form Ag MTPs and then transferred onto the nanoplate seeds via an Ostwald ripening process. Figure 11B shows TEM image of Ag nanoplates prepared using the seed-mediated growth for 4 h. To follow the growth process, we performed a set of syntheses and stopped them at various reaction times. Figure 11C shows UV−vis spectra of the as-prepared products as a function of the growth time. Similar to the spectra shown in Figure 1A, an isosbestic point was observed. This result indicates that the transformation from newly formed Ag MTPs (with an LSPR at 400 nm) to nanoplates. Specifically, oxidative etching of MTPs allowed the growth of Ag nanoplates from 50 to 100 nm in edge length. Taken together, we were able to use simple reduction of $AgNO_3$ by PVP-29K in ethanol under a solvothermal condition to tailor the optical properties of resultant Ag nanoplates in the both the visible to near-infrared regions.

Stability of Ag Nanoplates. Thermodynamically, Ag nanoplates with sharp corners have an inclination to spontaneously evolve into truncated plates with lower surface energies. For example, they were found to evolve into circular disks when aged in DI water at room temperature.[46] A number of groups also reported that this transformation could be accelerated when the samples were subjected to heating or ultraviolet irradiation.[47,48] This shape instability greatly affects the remarkable optical properties of Ag nanoplates. It was shown that the strong, in-plane dipole LSPR mode could shift its position by as much as 300 nm from the near-infrared to the blue region during the truncation of their sharp corners.[42] It is worth pointing out that this shape instability likely arises from the popular use of citrate in the synthesis of Ag nanoplates.

We also used UV−vis spectroscopy to evaluate the stability of the Ag nanoplates in ethanol. Specifically, we monitored the variations to the UV−vis spectra of an ensemble of Ag nanoplates to scrutinize any alterations to their LSPR peaks due to changes to their shape, size, and aggregation state. We examined two batches of Ag nanoplates that were prepared using the standard solvothermal synthesis in ethanol at 80 °C for 2 and 4 h, respectively. Figure 12 shows UV−vis spectra of the freshly prepared solutions and the same solutions after storage for 40 days. There are obvious changes to the peak at 400 nm and the shoulder peak at 650 nm for the sample that was prepared using a reaction time of 2 h, with MTPs in presence. In contrast, once the MTPs had been consumed completed and transformed into Ag nanoplates at a reaction time of 4 h, the sample showed no change to the LSPR peak at 750 nm over a period of 40 days. This result is consistent with our previous observation—MTPs were extremely susceptible to oxidative etching by the O_2 from air, leading to release of ionic Ag^+ ion and possible formation of new Ag nanoplates or growth of the existing Ag nanoplates into larger sizes. The ability to eliminate the MPTs in our solvothermal synthesis provides an opportunity to produce Ag nanoplates with remarkable stability in both shape and size.

4. CONCLUSIONS

We have demonstrated a robust method for the synthesis of Ag nanoplates with an edge length of 50 nm and conversion yield >99%. The synthesis simply involves the reduction of a Ag precursor ($AgNO_3$ or CF_3COOAg) by PVP in ethanol under a solvothermal condition at a temperature slightly higher than the boiling point of ethanol (80 vs 79 °C). When compared with the previously reported protocols, our approach only requires a Ag precursor, PVP, and ethanol to produce pure samples of Ag nanoplates, with no involvement of citrate and light irradiation. To understand the mechanism behind this facile and efficient synthesis, we investigated the effects of a number of reaction conditions, including the type of precursor, reducing power of PVP, molar ratio of PVP to $AgNO_3$, role of solvent, involvement of O_2, and other parameters associated with a solvothermal process (e.g., solution volume, pressure, and temperature). Collectively, our results support a mechanism that combines the following key features: quick chemical reduction of Ag^+ ions to generate Ag MTPs, kinetically controlled formation of plate-like seeds followed by their further growth into Ag nanoplates, and oxidative etching to promote Ostwald ripening for a complete transformation of Ag MTPs into nanoplates. In our synthesis, PVP played a critical role as the reducing agent. We also found that the molar ratio of PVP to $AgNO_3$, [PVP]/[$AgNO_3$], and the presence of ethanol were two important factors in controlling the reduction rate and thus for the formation of Ag nanoplates. For example, when [PVP]/[$AgNO_3$] was larger than 10:3, the reduction rate favored the formation of MTPs with sizes <10 nm and ultimately promoting a complete transformation from Ag MTPs to nanoplates with a conversion yield approaching 100%. In contrast, when a slower reduction was involved by either decreasing [PVP]/[$AgNO_3$] below the threshold of 5:3, replacing the PVP-29K with PVP-55K, or introducing DI water into the reaction system, larger MTPs were formed, together with an incomplete transformation of the Ag MTPs into nanoplates. Additionally, the presence of O_2 supported the Ostwald ripening process that dissolved MTPs into Ag^+ ions through oxidative etching, followed by the reduction of the Ag^+ ions into Ag atoms to ensure growth for the Ag nanoplates. It is worth noting that the solvothermal condition was essential to the reduction of $AgNO_3$ for producing Ag nanoplates with no MTPs as the byproduct. In particular, when the reaction temperatures were above the boiling point of ethanol, the pressure could accelerate the oxidative dissolution of MTPs and thus promote an efficient conversion of Ag MTPs into nanoplates. As a result, the reaction time of our solvothermal synthesis was much shorter than those that involved reduction under ambient pressure. This work not only offers a simple and reproducible route to the production of Ag nanoplates but also provides a comprehensive understanding of the experimental parameters that affect the formation of Ag nanoplates. The

insight put forth in this study can also be used to explain a number of previously reported syntheses of Ag nanoplates, such as those involving the thermal reduction of $AgNO_3$ by PVP or alcohols in an aqueous solution under ambient pressure. This study represents a step forward towards the optimization of solvothermal reaction with an exquisite control over the reduction kinetics to generate metal nanocrystals with different sizes and shapes.

■ ASSOCIATED CONTENT

Supporting Information

Figure S1 provides high-resolution TEM images of MTPs at the early stage of reaction with an average size less than 10 nm. Figure S2 shows a TEM image of Ag nanoplates synthesized by using AgCF3COO as a precursor to elemental Ag and the corresponding UV−vis spectrum. Figure S3 provides the corresponding UV−vis spectra of samples shown in Figure 4. Figure S4 includes TEM images and the corresponding UV−vis spectra of products that were synthesized by PVP-10K, PVP-29K, and PVP-55K, respectively. Figure 5S supports the role of ethanol and DI water in the synthesis of Ag nanoplates. This material is available free of charge via the Internet at http://pubs.acs.org.

■ AUTHOR INFORMATION

Corresponding Author

*E-mail: dong.qin@mse.gatech.edu.

Notes

The authors declare no competing financial interest.

■ ACKNOWLEDGMENTS

This work was supported in part by the start-up funds from the Georgia Institute of Technology and a NSF-NUE grant (Award EEC-1219512). Part of work was performed at the Institute of Electronics and Nanotechnology (IEN) at Georgia Institute of Technology, a member of National Nanotechnology Infrastructure Network, which was partially supported by NSF (Award ECS-0335765). Y.Y. and S.X. were also partially supported by the China Scholarship Council. We thank Professor Younan Xia at the Georgia Institute of Technology for helpful discussions.

■ REFERENCES

(1) Pastoriza-Santos, I.; Liz-Marzan, L. M. *J. Mater. Chem.* **2008**, *18*, 1724−1737.
(2) Millstone, J.E.; Hurst, S. J.; Metraux, G. S.; Cutler, J. I.; Mirkin, C. A. *Small* **2009**, *5*, 646−664.
(3) Rycenga, M.; Cobley, C. M.; Zeng, J.; Li, W. Y.; Moran, C. H.; Zhang, Q.; Qin, D.; Xia, Y. N. *Chem. Rev.* **2011**, *111*, 3669−3712.
(4) Kelly, K.; Coronado, E.; Zhao, L.; Schatz, G. C. *J. Phys. Chem. B.* **2003**, *107*, 668−677.
(5) Xue, C.; Mirkin, C. *Angew. Chem. Int. Ed.* **2007**, *46*, 2036−2038.
(6) Xue, C.; Metraux, G. S.; Millstone, J. E.; Mirkin, C. A. *J. Am. Chem. Soc.* **2008**, *130*, 8337−8344.
(7) Sherry, L. J.; Jin, R.; Mirkin, C. A.; Schatz, G. C.; Van Duyne, R. P. *Nano Lett.* **2006**, *6*, 2060−2065.
(8) Xia, Y.; Xiong, Y. J.; Lim, B.; Skrabalak, S. E. *Angew. Chem. Int. Ed.* **2009**, *48*, 60−103.
(9) Jin, R.; Cao, Y.; Mirkin, C.; Kelly, K. L.; Schatz, G.; Zheng, J. *Science* **2001**, *294*, 1901−1903.
(10) Jin, R. C.; Cao, Y. C.; Hao, E. C.; Metraux, G. S.; Schatz, G. C.; Mirkin, C. A. *Nature* **2003**, *425*, 487−490.
(11) Maillard, M.; Huang, P. R.; Brus, L. *Nano Lett.* **2003**, *3*, 1611−1615.
(12) Wu, X.; Redmond, P.; Liu, H.; Chen, Y.; Steigerwald, M.; Brus, L. *J. Am. Chem. Soc.* **2008**, *130*, 9500−9506.
(13) Chen, S.; Caroll, D. L. *Nano Lett.* **2002**, *2*, 1003−1007.
(14) Sun, Y.; Mayers, B.; Xia, Y. *Nano Lett.* **2003**, *3*, 675−679.
(15) Zhang, Q.; Ge, J.; Pham, T.; Goebl, J.; Hu, Y.; Lu, Z.; Yin, Y. *Angew. Chem., Int. Ed.* **2009**, *48*, 3516−3519.
(16) Sun, Y.; Xia, Y. *Adv. Mater.* **2003**, *15*, 695−699.
(17) Zeng, Jie.; Xia, X.; Rycenga, M.; Henneghan, P.; Li, Q.; Xia, Y. *Angew. Chem., Int. Ed.* **2011**, *50*, 244−249.
(18) Pastoriza-Santos, I.; M. Liz-Marzan, L. *Langmuir* **1999**, *15*, 948−951.
(19) Pastoriza-Santos, I.; M. Liz-Marzan, L. *Nano Lett.* **2002**, *2*, 903−905.
(20) Jiang, L. P.; Xu, S.; Zhu, J. M.; Zhang, J. R.; Zhu, J. J.; Chen, H. Y. *Inorg. Chem.* **2004**, *43*, 5877−5883.
(21) Washio, I.; Xiong, Y.; Yin, Y.; Xia, Y. *Adv. Mater.* **2006**, *18*, 1745−1749.
(22) Kim, M. H.; Lee, J. J.; Lee, J. B; Choi, K. Y. *CrystEngComm* **2013**, *15*, 4660−4666.
(23) Gentry, S. T.; Kendra, S. F.; Bezpalko, M. W. *J. Phys. Chem C.* **2011**, *115*, 12736−12741.
(24) Qian, Y. *Adv. Mater.* **1999**, *11*, 1101−1102.
(25) Rabenau, A. *Angew. Chem., Int. Ed.* **1985**, *24*, 1026−10.
(26) Yang, Y.; Matsubara, S.; Xiong, L.; Hayakawa, T.; Nogami, M. *J. Phys. Chem. B.* **2007**, *111*, 9095−9104.
(27) Lu, Q.; Lee, K. J.; Hong, S. J.; Myung, N. V.; Kim, H. T.; Choa, Y. H. *J. Nanosci. Nanotechnol.* **2010**, *10*, 3393−3396.
(28) Chen, D.; Qiao, X.; Qiu, X.; Chen, J.; Jiang, R. *J. Mater. Sci.: Mater. Electron.* **2011**, *22*, 6−13.
(29) Zeng, J.; Tao, J.; Li, W.; Grant, J.; Wang, P.; Zhu, Y.; Xia, Y. *Chem. Asian J.* **2011**, *6*, 376−379.
(30) Hofmeister, H.; Nepiko, S. A.; Levlev, D. N.; Schulze, W.; Ertl, G. *J. Cryst. Growth* **2002**, *234*, 773−781.
(31) Wiley, B.; Herricks, T.; Sun, Y.; Xia, Y. *Nano Lett.* **2004**, *4*, 1733−1739.
(32) Redmond, P. L.; Hallock, A. J.; Brus, L. E. *Nano Lett.* **2005**, *5*, 131−135.
(33) Gentry, S. T.; Kendra, S. F.; Bezpalko, M. W. *J. Phys. Chem. C.* **2011**, *115*, 12736−12741.
(34) Ledwith, D. M.; Whelan, A. M.; Kelly, J. M. *J. Mater. Chem.* **2007**, *17*, 2459−2464.
(35) Zhang, Q.; Cobley, C.; Au, L.; McKiernan, M.; Schwartz, A.; Wen, L.-P.; Chen, J.; Xia, Y. *Appl. Mater. Interfaces* **2009**, *1*, 2044−2048.
(36) Mdluli, P. S.; Sosibo, N. M.; Mashazi, P. N.; Nyokong, T.; Tshikhudo, R. T.; Skepu, A.; Lingen, E. *J. Mol. Struct.* **2011**, *1004*, 131−137.
(37) Xiong, Y.; Washio, I.; Chen, J.; Sadilek, M.; Xia, Y. *Angew. Chem., Int. Ed.* **2007**, *46*, 4917−4921.
(38) M. Liz-Marzan, L.; Lado-Tourino, I. *Langmuir* **1996**, *12*, 3585−3589.
(39) Pastoriza-Santos, I.; M. Liz-Marzan, L. *Langmuir* **2002**, *18*, 2888−2894.
(40) Kim, J.-S. *J. Ind. Eng. Chem.* **2007**, *13*, 566−570.
(41) Li, N.; Zhang, Q.; Quinlivan, S.; Goebl, J.; Gan, Y.; Yin, Y. *ChemPhysChem.* **2012**, *13*, 2526−2530.
(42) Zeng, J.; Robert, S.; Xia, Y. *Chem.—Eur. J.* **2010**, *16*, 12559−12563.
(43) Chen, S.; Fan, Z.; Carroll, D. L. *J. Phys. Chem. B* **2002**, *106*, 10777−10781.
(44) Brioude, A.; Pileni, M. P. *J. Phys. Chem. B.* **2005**, *109*, 23371−23377.
(45) Zhang, Q.; Li, W.; Moran, C.; Zeng, J.; Chen, J.; Wen, L. P.; Xia, Y. *J. Am. Chem. Soc.* **2010**, *132*, 11372−11378.
(46) Zeng, J.; Tao, J.; Su, D.; Zhu, Y.; Qin, D.; Xia, Y. *Nano Lett.* **2011**, *11*, 3010−3015.
(47) Tang, B.; An, J.; Zheng, X.; Xu, S.; Li, D.; Zhou, J.; Xu, W. *J. Phys. Chem. C* **2008**, *112*, 18361−18367.

(48) Zhang, Q.; Ge, J.; Pham, T.; Goebl, J.; Hu, Y.; Lu, Z.; Yin, Y. *Angew. Chem., Int. Ed.* **2009**, *48*, 3516−3519.